TISSUE ENGINEERING: Part C
Volume 22, Number 2, 2016

DOI: 10.1089/ten.tec.2015.0328

termis
Tissue Engineering
& Regenerative Medicine
International Society

METHODS ARTICLE

The Impact of Prestretch Induced Surface Anisotropy on Axon Regeneration

Chun Liu, PhD,[1] Ryan Pyne, BS,[1] Jungsil Kim, PhD,[2] Neil Thomas Wright, PhD,[3] Seungik Baek, PhD,[3] and Christina Chan, PhD[1,4]

Nerve regeneration after spinal cord injury requires proper axon alignment to bridge the lesion site and myelination to achieve functional recovery. Significant effort has been invested in developing engineering approaches to induce axon alignment with less focus on myelination. Topological features, such as aligned fibers and channels, have been shown to induce axon alignment, but do not enhance axon thickness. We previously demonstrated that surface anisotropy generated through mechanical prestretch induced mesenchymal stem cells to align in the direction of prestretch. In this study, we demonstrate that static prestretch-induced anisotropy promotes dorsal root ganglion (DRG) neurons to extend thicker axon aggregates along the stretched direction and form aligned fascicular-like axon tracts. Moreover, Schwann cells, when cocultured with DRG neurons on the prestretched surface colocalized with the aligned axons and expressed P0 protein, are indicative of myelination of the aligned axons, thereby demonstrating that prestretch-induced surface anisotropy is beneficial in enhancing axon alignment, growth, and myelination.

Introduction

As a leading cause of disabilities worldwide, spinal cord injury (SCI) is characterized by an acute traumatic lesion of neural elements in the spinal canal, which results in temporary or permanent deficits in sensory and motor function.[1] Structurally, axon tracts in the spinal cord, composed of highly ordered and aligned bundles of axons, form complex networks of connectivity. After acute SCI, axons sprout briefly, but soon undergo growth arrest and retraction due to the lack of secreted growth factors from associated glial cells and neurite orientation or alignment within the scar tissue, which prevent the axons from crossing into the lesion site.[2,3] If the nerve's gap from an injury is large, the distal and proximal ends of the damaged nerves are unable to communicate efficiently, thereby deterring the regeneration process. Transplantation of Schwann cells (SCs) or olfactory ensheathing cells has been shown to induce axon regeneration to an extent, with partial recovery of motor and sensory functions as unorganized axon alignment leads to disordered regeneration.[4,5] Therefore, to persuade a sufficient number of regenerating axons to bridge the lesion site, it is necessary to have properly organized axonal alignment.

Biomaterials used to fabricate scaffolds and implantable substrates for nerve regeneration have been investigated for their ability to modulate mechanical cues such as substrate stiffness, topological features, and stretch to control neural cell growth and have shown potential in neural regeneration post SCI.[6–9] To elicit axon outgrowth from regenerating neurons, topological features have been reported as critical for providing contact guidance.[6,7,10] Consequently, a significant effort has been invested in developing techniques that induce axon alignment to promote neural regeneration. Topological guidance achieved through aligned fibers, channels, and patterning has facilitated axon alignment,[6,11] but was unable to increase the length and thickness of the axons.[12] Furthermore, when transplanted *in vivo*, axons encounter difficulties in penetrating through the scaffold channels due to formation of a reactive cell layer.[13,14]

Alternatively, gradually stretching the substrate at a constant rate has led to axon alignment in the stretch direction with increasing axon length over time.[15] Despite these promising results, translating these technologies into effective therapies remains elusive due to the complexity of the experimental setup. Therefore, alternative approaches for axonal regeneration are needed. Demonstration that anisotropic stress *in vivo* induces orientation and affects cell morphogenesis[16] inspired us to pursue an approach that capitalized on surface anisotropy based on static prestretch to facilitate axon regeneration for SCI repair.

[1]Department of Chemical Engineering and Materials Science, Michigan State University, East Lansing, Michigan.
[2]Department of Mechanical Engineering & Materials Science, Washington University, Saint Louis, Missouri.
Departments of [3]Mechanical Engineering and [4]Biochemistry and Molecular Biology, Michigan State University, East Lansing, Michigan.

We previously demonstrated that the static prestretch creates surface anisotropy that influences cell alignment and growth.[12,17,18] While anisotropy is often attributed to the contact guidance provided by surface topography,[19–22] it differs from surface anisotropy. Briefly, the surface anisotropy can be generated through mechanical stretching, that is, prestretch, which we previously explored with polydimethyl-siloxane (PDMS) membranes to induce mesenchymal stem cells (MSCs) to express MyoD1. To predict the effective stiffness that the MSCs sense in the stretched direction, a finite elastic theory of ''small deformation superimposed on large''[23] was applied. The MSCs were able to sense the anisotropy by actively pulling on the surface and orienting in the prestretched direction.[17] In this study, we report axon alignment on a static prestretched PDMS substrate and show that static prestretch-induced surface anisotropy enhanced axon alignment, growth of dorsal root ganglion (DRG) neurons, and myelination of the axons by SCs. Both the DRG neurons and SCs are regularly used in clinical models of neural regeneration for SCI. DRG neurons have been demonstrated to survive upon clinical transplantation.[24–26] The roots of DRGs close to the lesion site are known to enter the spinal cord and extend processes across the host–graft interface.[27] DRG nerve constructs are amendable to nerve repair since their axons can lengthen extensively to bridge the lesion.[28] SCs can migrate to the SCI to promote neural repair and myelinate the regenerated axons.[29]

We designed a static prestretched cell culture system that provided surface anisotropy without topological features, enabling DRG neurons to extend thicker axon aggregates along the stretched direction and form aligned fascicular-like axon tracts. Moreover, the SCs aligned and colocalized with the aligned axons and expressed P0 protein, a marker for mature SCs and an indicator of myelination, thereby demonstrating that surface anisotropy is beneficial in enhancing axon alignment, growth, and myelination. We also compared the effect of stretch-induced anisotropy with that of topography-induced anisotropy. Although axons from cultured DRG neurons showed alignment on micropatterned PDMS channels, the axons in the channels do not form neatly aligned axon tracts or increase their thickness as on the prestretched surface, indicating an advantageous effect of prestretch-induced anisotropy on regenerating axon growth.

Materials and Methods

Materials

PDMS substrates were prepared using a 184-silicone elastomer kit purchased from Dow Corning (Midland, MI). A FlexiPERM ConA Silicone chamber was purchased from Greiner Bio-one (Monroe, NC). Poly-L-Lysine was purchased from Trevigen (Gaithersburg, MD). Poly-D-Lysine, fluoro-2 deoxy-uridine, uridine, cytosine β-D-arabinofuranoside (AraC), Anti-Thy 1.1 antibody (cat. no. M-7898), and Rabbit Complement were purchased from Sigma-Aldrich (St. Louis, MO). Heat-inactivated fetal bovine serum was purchased from Hyclone (Logan, UT). Bovine pituitary extract was purchased from Clonetics (Allendale, NJ). Forskolin was purchased from Calbiochem (Billerica, MA). Type I collagenase was purchased from Worthington (Lakewood, NJ). The neurobasal medium 1×, B-27 supplement, Glutamax-I, Albumax-I, nerve growth factor, Dulbecco's Modified Eagle Medium, penicillin, streptomycin, 0.25% trypsin-EDTA, 1×-phosphate-buffered saline (PBS), HEPES buffer, and immunostaining components (mouse anti-β-III tubulin antibody [cat. no.4466], Alexa Fluor 488 goat anti-mouse IgG secondary antibody, Alexa Fluor 546 goat anti-rabit IgG secondary antibody, and DAPI) were purchased from Invitrogen (Carlsbad, CA). Bovine serum albumin (BSA) was purchased from US Biological (Marblehead, MA). Rabbit anti-myelin protein zero antibody (cat. no. ab31851) was purchased from Abcam (Cambridge, MA).

Prestretched PDMS substrate preparation

Each PDMS substrate was cured in polystyrene tissue culture dish by mixing a 10:1 solution of base and curing agent with the mixture in the dish at 1-mm thickness. The mixture was kept under vacuum for 20 min to remove air bubbles and then cured overnight at 60°C. The PDMS surface was further cleaned with a PX-250 plasma cleaning/etching system (March Instruments, Freehold, NG) for 3 min at 165 mTorr and 65 sccm flow of O_2. A piece of rectangle PDMS membrane (5 × 3.5 cm) was fixed on the stretching frame and the frame was then placed on the stretching stage. The membrane was stretched evenly with 10% elongation in the longer axis, and the stretch was fixed (Fig. 1a). A silicone chamber was placed on top of the PDMS membrane, which provided a circular well to hold the culture medium. The entire device design is shown in Figure 1a. Before seeding the DRG neurons, 1.5 mL of poly-L-lysine (PLL) was added to the PDMS membrane and incubated for 2 h within the chamber to enhance cell attachment.

PDMS channel substrate preparation

Different size (50 and 200 μm) channel patterns were designed with equally sized grooves and ridges using AutoCAD. Photolithography was used to fabricate the micropatterned silicon wafers that served as molds to transfer the microgrooves on PDMS substrates as described previously.[30] PDMS substrates of 10:1 mixed base and curing agent were cured at 60°C overnight. PLL was subsequently added to the chamber and incubated for 2 h before seeding the DRG neurons.

PDMS surface characterization

Surface topography was analyzed by a scanning electron microscope (JSM-7500F cold field emission SEM, JEOL Corporation) in the secondary electron imaging mode. An acceleration voltage of 12 kV was used for all experiments. Images were taken at a magnification of 1500×.

Tensile test

The mechanical properties of the substrate (i.e., PDMS membrane) were measured by the uniaxial tensile test, and the mechanical behavior was described by the incompressible, isotropic neo-Hookean model described previously.[31]

DRG neuron and SC isolation and culture

All procedures for cell isolation were approved by the Institutional Animal Care and Use Committee at Michigan State University.

DRG neurons are isolated from 5- to 8-day-old Sprague-Dawley rats. Briefly, after sacrificing the pups by decapitation, the skin overlying the spinal cord is cut away and any excess tissue is removed from the spinal cord. The spine is then completely removed from the body, and the spinal cord is extracted. Using a fine pair of tweezers and a pair of microsurgery scissors, ~10–16 DRGs are collected from both sides, trimmed of nerve roots, and transferred to 5 mL of ice-cold HBSS buffer containing 1 mL penicillin/streptomycin. The dissection medium containing DRGs are then transferred into a new 15-mL tube and centrifuged at 900 RCF at 4°C for 5 min. After centrifugation, the supernatant is removed and the DRGs are incubated in 6 mL of 0.05% Trypsin-EDTA (1×) (Sigma; 1 mg/mL, 45 min) at 37°C and followed by 2 mL collagenase (Sigma; 500 U/mL, 20 min) at 37°C. After chemical dissociation, the ganglia are centrifuged at 900 RCF in 4°C for 5 min and the supernatant is subsequently removed. The pellet is further resuspended in 10 mL of standard growth media and centrifuged, as described above. After washing with the medium, the cells are resuspended in standard growth media containing the Neurobasal-A medium containing B-27 supplement, antibiotic (penicillin/streptomycin), Albumax-I, and nerve growth factor. The dissociated neurons are then plated on the PLL-coated prestretched surface and incubated at 37°C at 5% CO_2.

SCs are isolated using the same protocol as described previously.[32] One-day-old pups are sacrificed by decapitation. The sciatic nerves are then extracted by making an incision from the tail up the spine to the inner thigh near the foot. Nerve sections are cut into small pieces and transferred into a dissociation medium containing collagenase and trypsin and incubated for 45 min at 37°C. Mechanical dissociation is done using an 18-gauge needle and 10-mL syringe. Cells are then centrifuged for 5 min and resuspended in Dulbecco's modified medium E containing 10% fetal bovine serum and 1% antibiotic (penicillin/streptomycin). Purification begins upon adding AraC into the medium after 48 h of culture, followed by antibody selection using Anti-thy 1.1 antibody and Rabbit Compliment on day 5.

The coculture of DRG neurons and SCs was performed after 2 weeks of culture of purified DRG neurons on stretched and unstretched surfaces by adding the SCs to the DRG culture at a cell density of 5000 cells/mL. The coculture was maintained for 1 week and then subjected to immunostaining.

Immunocytochemistry

Immunocytochemistry was performed at room temperature on cells seeded on the stretched surface for 6, 12, and 21 days. Cells were rinsed with PBS, followed by fixation with 4.0% paraformaldehyde in PBS for 15 min, rinsed thrice in PBS, then permeabilized with 0.1% Triton X-100 in PBS for 15 min, and washed thrice with PBS. After washing, the cells were blocked in 1% BSA for 30 min. After BSA blocking, the cells were incubated with mouse anti-mouse β-III tubulin primary antibody (1 μL stock per 500 μL of 1% BSA solution) for 1 h, or rabbit anti-P0 primary antibody (1:500 dilution in 1% BSA solution) for 1 h followed by three washes in 1× PBS, and then incubated with Alexa Fluor 488 goat anti-mouse or anti-rabbit Alexa Flour 546 secondary antibody (1:500 dilution in 1% BSA solution) for 1 h. Cells were washed again, thrice in 1× PBS, and then incubated for 5 min in 300 nM DAPI to visualize the nucleus. The PDMS substrates were air dried and the silicone chamber was removed from the membrane; the stained PDMS membrane was finally kept in the dark to cure for 24 h at room temperature. Confocal laser scanning microscopy images were obtained with Olympus FluoView1000 laser scanning confocal microscope using 20× objectives.

Quantification of axon orientation distribution and axon thickness

Image-Pro Plus version 4.5 was used to measure the axon orientation angles. Briefly, before measurements, the fluorescent images were converted into high-contrast binary images to remove the background noise. A straight line was drawn perpendicular to the stretch direction, which was used as the reference to indicate zero degree orientation. For each axon, the orientation was measured by drawing a straight line to follow the axon pathway, and the angle between the traced line and the reference line was automatically given by the software and recorded for further analysis. All experiments were repeated at least thrice for statistical verification. For the stretched versus unstretched comparison, the DRG neurons seeded on the stretched and unstretched membranes were from the same isolation. For each experiment, we took eight images under the same condition and quantified the axon orientation angles. We counted the axons at each 10° of orientation and normalized the number to the total number of axons in each condition. For axon thickness analysis, we enlarged each image by 10× and measured the axon thickness by pixels, which were later converted into microns. The mean value and standard deviation of the axon thickness were reported.

Quantification of colocalization of axon and SCs

The fluorescent images of the coculture were processed by setting the threshold of each color channel to remove background noise, and the colocalization was automatically quantified using the FV1000 software. The percentage of green that overlapped with red was calculated for both the stretched and unstretched surfaces. For statistical analysis, three biological samples were quantified, with six images analyzed for each sample.

Statistical analyses

Data are expressed as mean ± standard deviation. A two-sample Kolmogorov–Smirnov test was applied to evaluate the statistical significance for Figure 3. A two-sample Student's *t*-test was used to determine statistical significance for Figure 4 and Figure 6e. The ANOVA-Tukey's test was applied to assess for significance in Figure 5. In all cases, *p*-values of <0.05 were considered statistically significant.

Results and Discussion

Design and characterization of prestretched surface

Using a previously designed cell culture system that induced alignment of MSCs, we explored how surface anisotropy affects axon alignment and growth. The cell culture

system is composed of a PDMS membrane fixed on a sliding frame and placed on a stretching stage used to control the magnitude of prestretch (Fig. 1a). The DRG neurons were seeded subsequent to stretching the PDMS substrate, that is, substrate prestretch, ensuring no other external forces were applied to influence the axon growth.

To ensure that there were no topographical features on the prestretched PDMS substrates that might affect axon alignment, for example fibers, the surface was imaged with the secondary electron imaging mode in SEM. SEM images of prestretched (Fig. 1bi and 1bii) and unstretched (Fig. 1biii and 1biv) surfaces, both with (Fig. 1bii and 1biv) and without PLL coating (Fig. 1bi and 1biii), showed that the stretch did not induce any topological features on the PDMS substrate (Fig. 1bi and 1biii). The dehydrating imaging condition caused the PLL peptides to aggregate into large particles on the membrane surface (Fig. 1bii and 1biv). Nonetheless, both surfaces, including the PLL-coated surface, show a smooth background without any surface topography (i.e., orienting features) that would provide contact guidance for axon alignment.

A nonlinear parameter estimation method was used to fit a neo-Hookean model to the results of a uniaxial tensile test of the PDMS substrate. The material behavior shows a linear elastic behavior up to a strain of 0.2 as shown in the left panel in Figure 1c. A prestretch value of 0.1 (10%) was used in the experiments. The left panel in Figure 1c shows the experimental data of the Cauchy stress versus engineering strain for the 10:1 cross-linked PDMS membrane, while the middle panel compares the model with the measured values of the engineering stress as a function of the engineering strain. See our previous study[33] for details on the parameter estimation using a finite elastic constitutive model.

The stretch-induced anisotropy of the PDMS membrane is represented by the ratio of effective stiffness in the stretched direction to its perpendicular direction (i.e., $\hat{E}_{1111}/\hat{E}_{2222}$). The effective stiffness in both directions with respect to the change in strain is shown in the right panel in Figure 1c. When there is no stretch, $\hat{E}_{1111} = \hat{E}_{2222}$ (1.45 MPa), which provides the elastic modulus of the 10:1 cross-linked PDMS membrane. As the stiffness in the stretched direction increases, the stiffness in the perpendicular direction decreases as the PDMS membrane experiences more strain during the uniaxial stretch. The predicted anisotropy of the PDMS membrane under a 5% strain is $\sim$1.158.

Axon alignment on prestretched surface

The DRG neuron cell suspension added to the chamber on the prestretched PDMS substrate was cultured for 6, 12, and 21 days to assess for DRG axon alignment. To examine axon growth, the cells on the prestretched and unstretched PDMS substrates were stained for β-III-tubulin (Fig. 2). The DRG axons on the prestretched surface aligned parallel to

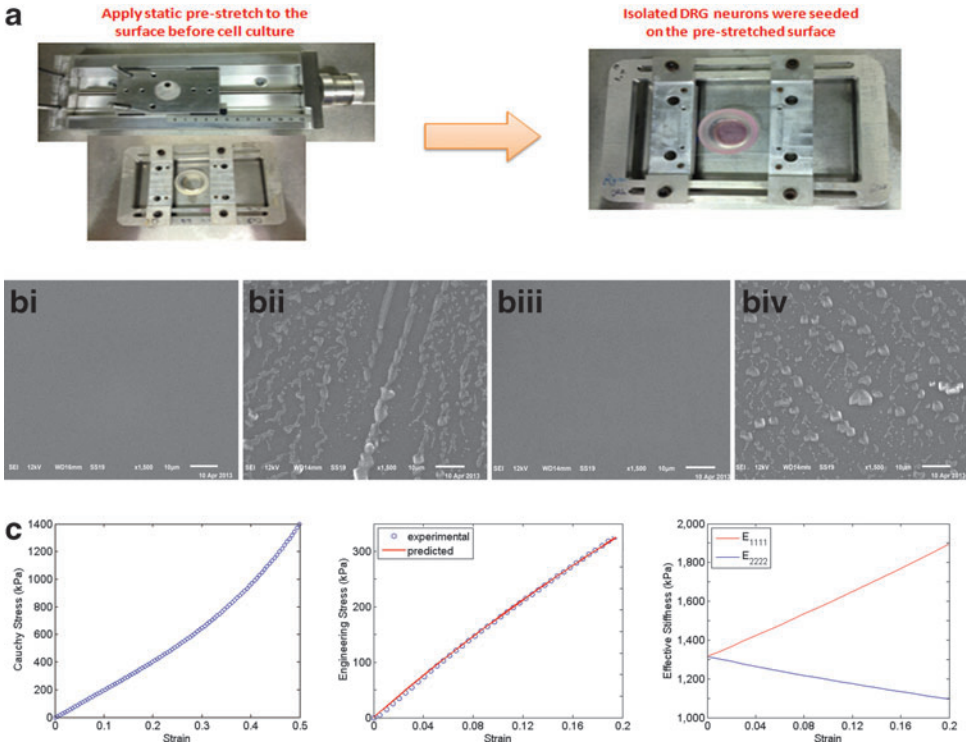

FIG. 1. Prestretched PDMS substrate and surface characterization. **(a)** PDMS membrane was placed on the stretching frame, and after the stretch was selected and secured, the DRG neurons were seeded on the chamber; **(b)** scanning electron microscope images of prestretched **(bi** and **bii)** and unstretched **(biii** and **biv)** PDMS surface with **(bii** and **biv)** and without **(bi** and **biii)** PLL coating; and **(c)** stretch–strain plot and effective stiffness curve. Tensile test was performed on the 10:1 cross-linked PDMS membrane and the true stress–strain curve is shown for one of the samples in the *left panel*. A neo-Hookean was used to fit the experimental data in the *middle panel*, and the predicted effective stiffness in both the stretch and perpendicular directions is depicted in the *right panel*. DRG, dorsal root ganglion; PDMS, poly-dimethyl-siloxane. Color images available online at www.liebertpub.com/tec

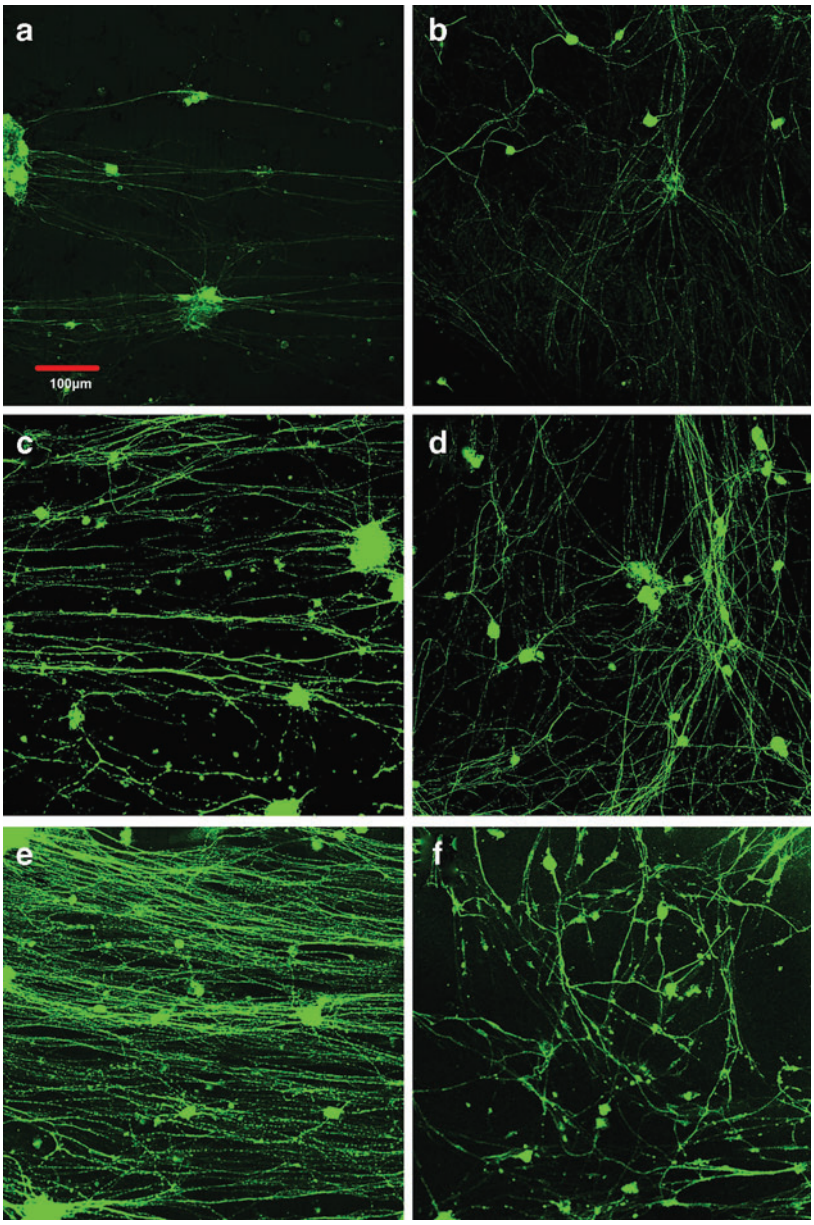

FIG. 2. Axon alignment on prestretched and unstretched surface. Fluorescent images of DRG neurons seeded on the static prestretched surface for **(a)** 6, **(c)** 12, and **(e)** 21 days, compared with DRG cells seeded on the unstretched surface for **(b)** 6, **(d)** 12, and **(f)** 21 days. Axons were stained with anti-mouse β-III tubulin and imaged with confocal microscopy (10×). Color images available online at www.liebertpub.com/tec

the stretched direction, while the axons on the unstretched surface aligned randomly and formed interconnected network. The axons on the prestretched substrate increased their alignment over time and formed longer and thicker fascicular axon tracts, which resembled the *in vivo* nervous systems. The prestretch-induced axon alignment was quantified and compared with the axons on the unstretched substrates according to the orientation angle (Fig. 3), where 90° is parallel to the prestretched direction and has the highest effective stiffness. The axon alignment was quantified by determining the percentage of axons that aligned at 10° intervals. The pyramid shape of the bar graph is maintained over time on the stretched substrate, indicating that the percentage of axons that aligned remained constant. In contrast, the axons on the unstretched surface did not align. The distribution of cell orientation on the unstretched surface was statistically different than on the stretched samples based on a two-sample Kolmogorov–Smirnov test on days 6, 12, and 21 (p-values are 0.001, 0.002, and 0.001, respectively).

This observation is in agreement with our previous report of MSC alignment on prestretch-induced anisotropic surface, which can be explained by the theory of active sensing. A possible explanation for the alignment of the DRG is that neurons can generate forces through the growth cone to sense the substrate stiffness.[9,34] Growth cones can actively generate forces and sense the substrate stiffness and thus may be sensing the higher effective stiffness in the prestretched direction leading to its alignment in the direction of maximum effective stiffness.

During the development and regeneration of the nervous system, neuronal growth cones navigate through tissues and experience environments with different mechanical properties established by the cytoarchitecture of the nervous tissue and surrounding tissues.[35] Koch *et al.* previously showed that the growth cones of DRG neurons generate extensive

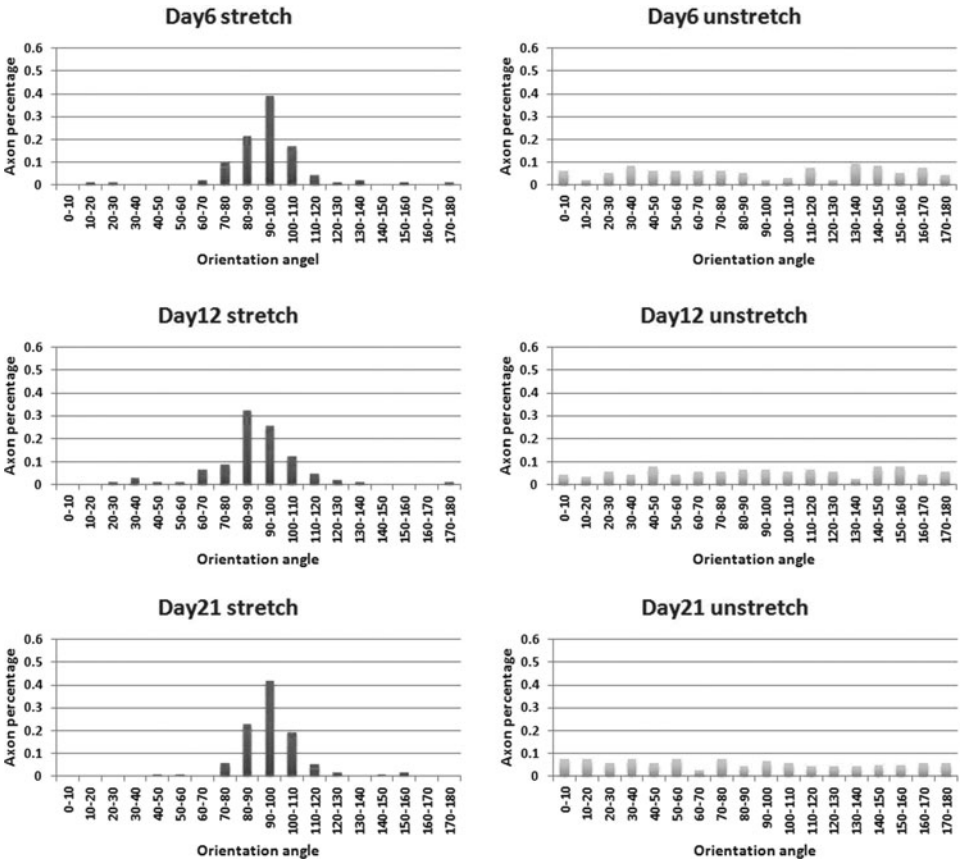

FIG. 3. Quantification of axon alignment on stretched versus unstretched PDMS substrate. Ratio of DRG axon alignment at every 10° on the prestretched and unstretched surfaces after 6, 12, and 21 days, with 90° representing the direction of the prestretch. Orientation angles were quantified by ImagePro Plus. Two-sample Kolmogorov–Smirnov test was applied to evaluate the statistical significance. The cells on the unstretched surface compared to the cells on the corresponding stretched samples for 6, 12, and 21 days have statistically different distributions, $p = 0.001$, 0.002, and 0.001, respectively.

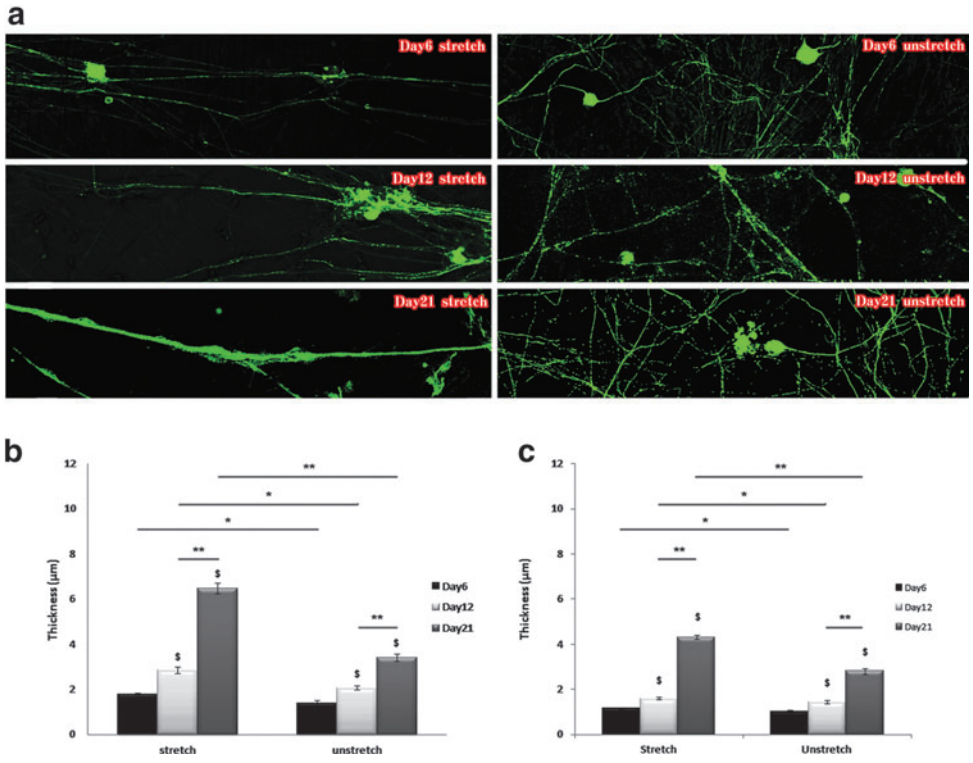

FIG. 4. Axon thickness growth on stretched versus unstretched PDMS substrate. **(a)** Fluorescent images of the DRG axons on the stretched (*left*) and unstretched (*right*) surfaces after 6 (*top*), 12 (*middle*), and 21 (*bottom*) days. Axons were stained with anti-mouse β-III tubulin and imaged with confocal microscopy (10×); **(b)** quantification of DRG axon bundle thickness on the prestretched and unstretched surfaces after 6, 12, and 21 days; and **(c)** quantification of single DRG axon thickness on the prestretched and unstretched surfaces after 6, 12, and 21 days. $^{\$}p < 0.01$, $^{*}p < 0.05$, $^{**}p < 0.01$. Color images available online at www.liebertpub.com/tec

traction force during axon extension, which is strongly dependent on the substrate stiffness.[34] The contractile forces that growth cones exerted have been associated with filopodia.[36] Thus, the axon alignment on the prestretched surface is potentially due to the active sensing by growth cones. Similar to MSCs, the filopodia of the growth cone actively pull on the substrate through binding sites, allowing cells to sense the difference in effective stiffness of the substrate in different directions.[37] This could cause the growth cone to move in the direction of maximum effective stiffness. In the present study, both the prestretched and unstretched substrates were coated with PLL and showed no topological features (Fig. 1b), ensuring that the axon alignment was due to the prestretch-induced anisotropy. Taken together, these results suggest that active cell sensing is likely to explain the axon growth.

Enhanced axon thickness growth on prestretched surface

In addition to inducing axon alignment, the prestretch-induced anisotropy appeared to enhance the fasciculation of axons. The aligned axons on the stretched surface formed thick clusters, which is quite different from the random axon network on the unstretched surface. The axons on the prestretched substrate grew thicker over time (Fig. 4a), with some aggregates forming clusters that appear similar to fascicular tracts. To evaluate this fascicular-like effect on the prestretched surface, we measured the thickness of each single unit of axon in the images, where the unit might contain individual or multiple aggregated axons, which were not easily distinguishable. The axon cluster thickness on both the stretched and unstretched surfaces on days 6, 12, and 21 increased over time. However, the average axon cluster thickness after 21 days of culture on the stretched surface was 1.5 times greater than on the unstretched surface, suggesting that the anisotropic-prestretched surface has the potential to promote extensive axon growth.

Since axon alignment is a prerequisite for fascicle formation,[38] the alignment might also be facilitating the fascicular-like effect observed on the prestretched surface. This fascicular-like effect has also been observed to increase on a gradually increasing stretching device, where axons were stretched daily using a stepper motor,[15] similar to what was observed in this study. However, the quantification in Figure 4b was a combined effect of both fascicular-like

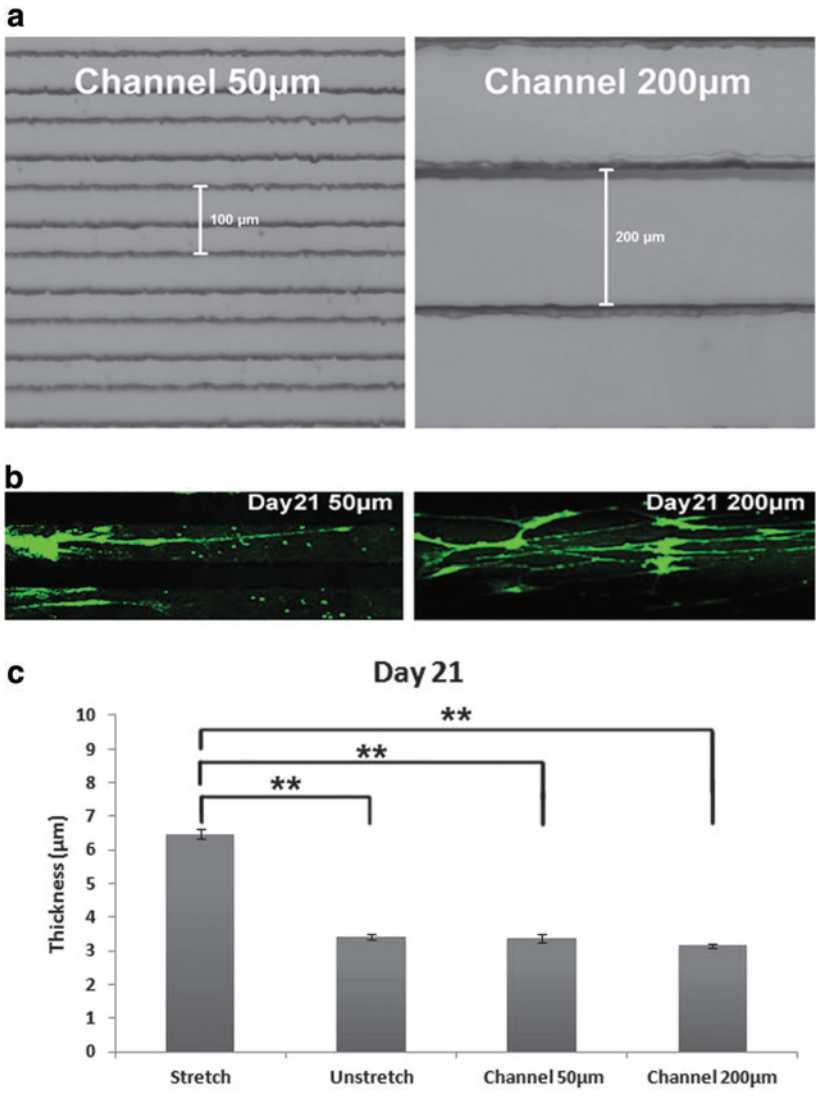

FIG. 5. Quantification of axon thickness on micropatterned PDMS substrate. **(a)** Phase-contrast images (10×) of micropatterned channels of 50 µm (*left*) and 200 µm (*right*) widths; **(b)** DRG axons on channels of 50 µm (*left*) and 200 µm (*right*) widths after 21 days of culture were stained with anti-mouse β-III tubulin and imaged with confocal microscopy (20×); and **(c)** comparison of axon thickness on the channels versus on the prestretched PDMS substrate after 21 days of culture. ANOVA-Tukey's test was applied to assess for significant difference. $^{**}p < 0.01$. Color images available online at www.liebertpub.com/tec

tracts and single axon thickness increase. Thus, to differentiate between the fascicular-like tracts and single axons, we selected the 10 thinnest axon units on the stretched and unstretched surfaces in each image and measured their thicknesses and found that the mean single axon thickness on the prestretched surface was significantly larger than that on the unstretched surface (Fig. 4c). The average thicknesses of the single axons grew over time and were 1.17, 1.60, and 4.31 μm on the prestretched surfaces and 1.01, 1.43, and 2.80 μm on the unstretched surface after 6, 12, and 21 days of culture, respectively. The results on the unstretched surfaces are in agreement with the 2–3 μm axon diameter reported in the CNS, which includes those in the brain that are typically thinner than in the spinal cord,[39,40] indicating that the unstretched surface did not hamper the growth of axons. The axon thickness on the prestretched surface is similar to the mean diameters of 4.18 and 5.95 μm reported, respectively, for myelinated sensory axon proximal and distal to lumbosacral dorsal root ganglia,[41] which are known to be the thickest axons in the CNS. Therefore, the prestretch-induced anisotropic surface not only enhances fascicular-like tract formation but also increases single axon thickness.

Axon alignment, given its significance in neural regeneration, has been extensively investigated.[13,21,42–44] Topological features such as fibers and channels provide contact guidance and are commonly used to guide axon extension along the surface topography. There has been no study, to date, which demonstrated that topological contact guidance induces both increases in axon thickness and a fascicular-like effect. To test this, we further cultured DRG neurons for 21 days on micropatterned channel surfaces of 50 and 200 μm, wherein the ridges and channels were of equal dimensions (Fig. 5a). The contact guidance induced by the channels causes the axons to align to some extent (Fig. 5b), however, the thicknesses of the axons on the channels were

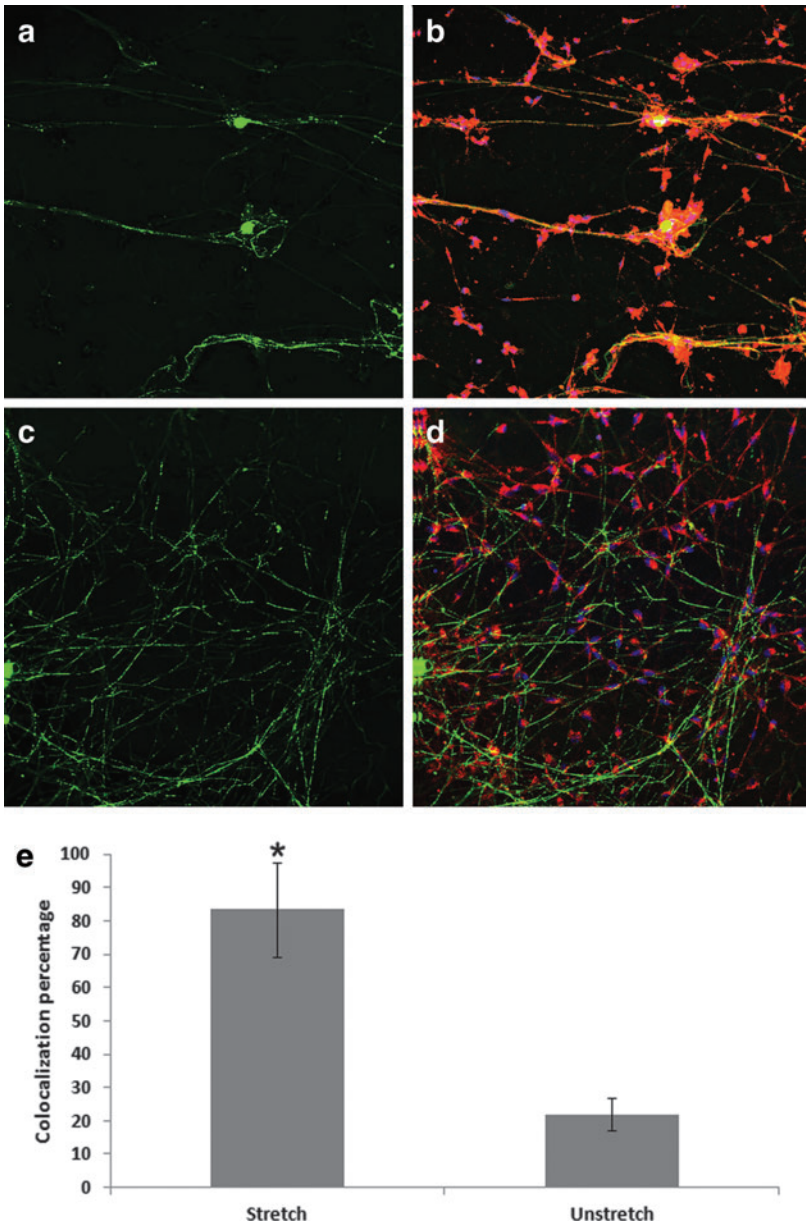

FIG. 6. Coculture of SCs with the DRG neurons on the stretched versus unstretched PDMS substrates. After culturing the DRG neurons on the stretched and unstretched surfaces for 2 weeks, purified SCs were added to the chamber and cultured for another week. **(a)** β-III-tubulin (*green*) staining of axons on the stretched PDMS substrate; **(b)** overlay of β-III-tubulin (*green*), P0 (*red*), and DAPI (*blue*) staining on the stretched substrate; **(c)** β-III-tubulin (*green*) staining of axons on the unstretched substrate; and **(d)** overlay of β-III-tubulin (*green*), P0 (*red*), and DAPI (*blue*) staining on the unstretched substrate. **(e)** Quantification of colocalization of β-III-tubulin (*green*) with P0 (*red*), the percentage of area in *green* color that was overlapped with *red* color was quantified using FV1000 software and shown as bar graph for stretched and unstretched surfaces. $*p < 0.01$. SC, Schwann cell. Color images available online at www.liebertpub.com/tec

significantly smaller than on the prestretched surface (Fig. 5c), suggesting that the prestretch-induced anisotropy could be more effective for enhancing axon growth for neural regeneration.

The exact mechanism of this prestretch-induced axon thickening and fascicular-like effect is unclear. Evidence suggests, however, that microtubules may be involved in this process.[45] There are three main filamentous components inside axon tubular structures, including microtublues, neurofilaments, and the microtrabecular matrix.[46,47] Although there have been studies that showed neurofilaments are responsible for providing mechanical strength, a recent study suggests that microtubules contribute a majority of the mechanical stiffness to the axons.[48] Previous studies indicate that mechanical tension facilitates growth of the axon, which may be associated with tensile loading of the microtubule bundle and subsequent growth. Microtubules have been suggested as mechanical force sensors that can detect the force direction and magnitude.[45,49,50] Axons on the prestretch surface showed more β-III-tubulin, a marker of microtubule components, indicating thicker axons, thereby raising a possibility that the prestretch might impact microtubule dynamics. Future experiments are needed to determine whether the prestretch-induced surface anisotropy signals microtubule polymerization to cause the axonal thickening observed.

Coculture of SCs with aligned axons

SCs are able to migrate into areas of damaged central nervous system and remyelinate the demyelinated axons.[51] Since myelination is dependent on the axon thickness and thicker axons are preferentially myelinated, SCs were cocultured on stretched and unstretched surfaces with 2-week-old cultured and aligned DRG axons for a week (Fig. 6). The axons were stained for β-III tubulin, while the SCs were stained for P0, an indicator of myelination. P0 is a marker of mature SCs and is a component of the myelin sheath. Significant colocalization of green (β-III tubulin) and red (P0) fluorescence occurred on the stretched surface (Fig. 6b), while on the unstretched surface, the red and green fluorescence did not colocalize significantly (Fig. 6d), The colocalization of β-III tubulin and P0 is quantified in Figure 6e, where the vertical axis represented the percentage of green fluorescence that overlapped with red fluorescence. From Figure 6e, the percentage of red and green fluorescence colocalized on the prestretched surface was $\sim$80%, indicating that the SCs attached and aligned with the axons. In contrast, the percentage of colocalization on the unstretched surface was around 25%, indicating β-III tubulin and P0 did not colocalize significantly on the unstretched surface (Fig. 6d). Therefore, as demonstrated in Figure 6, the prestretched surfaces enhanced not only axon alignment and fascicular-like tract formation but also increased the attachment of SCs to the aligned axons, a requisite for myelination.

Many studies, using topological features or motor stretch, demonstrated that axons can be induced to align, but they did not explore myelination on the aligned axons.[52–55] Although myelination has been shown with SCs and DRG neuron cocultures, the myelination results in the previous study were achieved by adding growth factors.[56] Oligodendrocytes myelinated axons on randomly oriented electrospun nanofibers of 0.4 μm thickness or larger,[57] in contrast, the aligned axons on the prestretched surface shown in this study not only myelinated but also formed thicker axons, all of which are important for nerve regeneration after SCI. Recently, Xia *et al.* demonstrated that aligned PMMA nanofibers can enhance the colocalization of DRG neurons with SCs, however, they did not measure myelination.[11] In contrast, our study using P0 staining of SCs clearly indicates myelination of the aligned axons and suggests that the prestretched anisotropic surface is capable of enhancing myelination. In contrast, the SCs on the unstretched substrate also stained positive to P0, but with minimal colocalization with β-III tubulin, demonstrating that the axons were not myelinated. The alignment and attachment of the SCs to the axons suggest enhanced myelination on the prestretched substrate and is likely due to the combined effect of both axon alignment and increased axon thickness. Thus, the ability of prestretch-induced anisotropic surfaces to guide attachment of SCs to aligned axons suggests that surface anisotropy could be capitalized upon to enhance myelination of endogenous axons.

Acknowledgments

This study was supported, in part, by the National Science Foundation (CBET 0941055 and CBET 1148298), the National Institutes of Health (R21CA176854, R01GM089866, and R01EB014986). We thank Dr. Melinda Frame from the Center for Advanced Microscopy at Michigan State University for help with confocal microscopy imaging. We thank Aritro Nath and Xiaopeng Bi for their assistance with the Kolmogorov–Smirnov test and photolithography, respectively, at Michigan State University.

Disclosure Statement

No competing financial interests exist.

References

1. Tohda, C., and Kuboyama, T. Current and future therapeutic strategies for functional repair of spinal cord injury. Pharmacol Ther **132,** 57, 2011.
2. Sorensen, A., Alekseeva, T., Katechia, K., Robertson, M., Riehle, M.O., and Barnett, S.C. Long-term neurite orientation on astrocyte monolayers aligned by microtopography. Biomaterials **28,** 5498, 2007.
3. Stocum, D.L. Regeneration of neural tissues. In: Regenerative Biology and Medicine (Second Edition). San Diego, CA: Academic Press, 2012, pp. 67–97.
4. Li, Y., Field, P.M., and Raisman, G. Repair of adult rat corticospinal tract by transplants of olfactory ensheathing cells. Science **277,** 2000, 1997.
5. Geller, H.M., and Fawcett, J.W. Building a bridge: engineering spinal cord repair. Exp Neurol **174,** 125, 2002.
6. Berns, E.J., Sur, S., Pan, L.L., Goldberger, J.E., Suresh, S., Zhang, S.M., Kessler, J.A., and Stupp, S.I. Aligned neurite outgrowth and directed cell migration in self-assembled monodomain gels. Biomaterials **35,** 185, 2014.
7. Chua, J.S., Chng, C.P., Moe, A.A.K., Tann, J.Y., Goh, E.L.K., Chiam, K.H., and Yim, E.K.F. Extending neurites sense the depth of the underlying topography during neuronal differentiation and contact guidance. Biomaterials **35,** 7750, 2014.

8. Loverde, J.R., and Pfister, B.J. Parallels between axon stretch growth and regeneration following injury. J Neurotrauma **29,** A28, 2012.
9. Suter, D.M., and Miller, K.E. The emerging role of forces in axonal elongation. Prog Neurobiol **94,** 91, 2011.
10. Kidambi, S., Lee, I., and Chan, C. Primary neuron/astrocyte co-culture on polyelectrolyte multilayer films: a template for studying astrocyte-mediated oxidative stress in neurons. Adv Funct Mater **18,** 294, 2008.
11. Xia, H., Chen, Q., Fang, Y., Liu, D., Zhong, D., Wu, H., Xia, Y., Yan, Y., Tang, W., and Sun, X. Directed neurite growth of rat dorsal root ganglion neurons and increased colocalization with Schwann cells on aligned poly(methyl methacrylate) electrospun nanofibers. Brain Res **1565,** 18, 2014.
12. Mitchel, J.A., and Hoffman-Kim, D. Cellular scale anisotropic topography guides Schwann cell motility. PLoS One **6,** e24316, 2011.
13. Gros, T., Sakamoto, J.S., Blesch, A., Havton, L.A., and Tuszynski, M.H. Regeneration of long-tract axons through sites of spinal cord injury using templated agarose scaffolds. Biomaterials **31,** 6719, 2010.
14. Mehrotra, S., Lynam, D., Liu, C., Shahriari, D., Lee, I., Tuszynski, M., Sakamoto, J., and Chan, C. Time controlled release of arabinofuranosylcytosine (Ara-C) from agarose hydrogels using layer-by-layer assembly: an in vitro study. J Biomater Sci Polym Ed **23,** 439, 2012.
15. Smith, D.H. Stretch growth of integrated axon tracts: extremes and exploitations. Prog Neurobiol **89,** 231, 2009.
16. Lau, K., Tao, H., Liu, H.J., Wen, J., Sturgeon, K., Sorfazlian, N., Lazic, S., Burrows, J.T.A., Wong, M.D., Li, D.Y., Deimling, S., Ciruna, B., Scott, I., Simmons, C., Henkelman, R.M., Williams, T., Hadjantonakis, A.K., Fernandez-Gonzalez, R., Sun, Y., and Hopyan, S. Anisotropic stress orients remodelling of mammalian limb bud ectoderm. Nat Cell Biol **17,** 569, 2015.
17. Liu, C., Baek, S., Kim, J., Vasko, E., Pyne, R., and Chan, C. Effect of static pre-stretch induced surface anisotropy on orientation of mesenchymal stem cells. Cell Mol Bioeng **7,** 106, 2014.
18. Miller, E.D., Li, K., Kanade, T., Weiss, L.E., Walker, L.M., and Campbell, P.G. Spatially directed guidance of stem cell population migration by immobilized patterns of growth factors. Biomaterials **32,** 2775, 2011.
19. Ahmed, Z., and Brown, R.A. Adhesion, alignment, and migration of cultured Schwann cells on ultrathin fibronectin fibres. Cell Motil Cytoskeleton **42,** 331, 1999.
20. Hsu, S.H., Chen, C.Y., Lu, P.S., Lai, C.S., and Chen, C.J. Oriented Schwann cell growth on microgrooved surfaces. Biotechnol Bioeng **92,** 579, 2005.
21. Miller, C., Jeftinija, S., and Mallapragada, S. Micropatterned Schwann cell-seeded biodegradable polymer substrates significantly enhance neurite alignment and outgrowth. Tissue Eng **7,** 705, 2001.
22. Wang, H.B., Mullins, M.E., Cregg, J.M., McCarthy, C.W., and Gilbert, R.J. Varying the diameter of aligned electrospun fibers alters neurite outgrowth and Schwann cell migration. Acta Biomater **6,** 2970, 2010.
23. Baek, S., Gleason, R.L., Rajagopal, K.R., and Humphrey, J.D. Theory of small on large: potential utility in computations of fluid-solid interactions in arteries. Comput Methods Appl Mech Eng **196,** 3070, 2007.
24. Bauchet, L., Mille-Hamard, L., Baillet-Derbin, C., and Horvat, J.C. Transplantation of autologous dorsal root ganglia into the peroneal nerve of adult rats: uni- and bi-directional axonal regrowth from the grafted DRG neurons. Exp Neurol **167,** 312, 2001.
25. Kuhlengel, K.R., Bunge, M.B., and Bunge, R.P. Implantation of cultured sensory neurons and Schwann-cells into lesioned neonatal rat spinal-cord. I. Methods for preparing implants from dissociated cells. J Comp Neurol **293,** 63, 1990.
26. Rosario, C.M., Aldskogius, H., Carlstedt, T., and Sidman, R.L. Differentiation and axonal outgrowth pattern of fetal dorsal-root ganglion-cells orthotopically allografted into adult-rats. Exp Neurol **120,** 16, 1993.
27. Marwah, J., Teitelbaum, H., and Prasad, K.N. Neural Transplantation, CNS Neuronal Injury, and Regeneration. Boca Raton, FL: Taylor & Francis, 1994.
28. Pfister, B.J., Iwata, A., Taylor, A.G., Wolf, J.A., Meaney, D.F., and Smith, D.H. Development of transplantable nervous tissue constructs comprised of stretch-grown axons. J Neurosci Methods **153,** 95, 2013.
29. Khuong, H.T., and Midha, R. Advances in nerve repair. Curr Neurol Neurosci Rep **13,** 322, 2013.
30. Bi, X.P., and Li, W. Fabrication of flexible microlens array through vapor-induced room temperature dewetting on plasma treated Parylene-C. Engineering in Medicine and Biology Society (EMBC), 2014 36th Annual International Conference of the IEEE, Chicago, IL, 2014, pp. 2085–2088.
31. Liu, C., Baek, S., Kim, J., Vasko, E., Pyne, R., and Chan, C. Effect of static pre-stretch induced surface anisotropy on orientation of mesenchymal stem cells. Cell Mol Bioeng **7,** 106, 2014.
32. Mantuano, E., Jo, M., Gonias, S.L., and Campana, W.M. Low density lipoprotein receptor-related protein (LRP1) regulates Rac1 and RhoA reciprocally to control Schwann cell adhesion and migration. J Biol Chem **285,** 14259, 2010.
33. Zeinali-Davarani, J.C.S., and Baek, S. On parameter estimations for biaxial mechanical behavior of arteries. J Biomech **42,** 524, 2009.
34. Koch, D., Rosoff, W.J., Jiang, J.J., Geller, H.M., and Urbach, J.S. Strength in the periphery: growth cone biomechanics and substrate rigidity response in peripheral and central nervous system neurons. Biophys J **102,** 452, 2012.
35. Franze, K., and Guck, J. The biophysics of neuronal growth. Rep Prog Phys **73,** 1, 2010.
36. Heidemann, S.R., Lamoureux, P., and Buxbaum, R.E. Growth cone behavior and production of traction force. J Cell Biol **111,** 1949, 1990.
37. Neukirchen, D., and Bradke, F. Neuronal polarization and the cytoskeleton. Semin Cell Dev Biol **22,** 825, 2011.
38. Brushart, T.M., Mathur, V., Sood, R., and Koschorke, G.M. Dispersion of regenerating axons across enclosed neural gaps. J Hand Surg Am **20,** 557, 1995.
39. Waxman, S.G., and McDonald, W.I. Form and Function in the Brain and Spinal Cord: Perspectives of a Neurologist. Cambridge, MA: MIT Press, 2003.
40. Totoiu, M.O., and Keirstead, H.S. Spinal cord injury is accompanied by chronic progressive demyelination. J Comp Neurol **486,** 373, 2005.
41. Suh, Y.S., Chung, K., and Coggeshall, R.E. A study of axonal diameters and areas in lumbosacral roots and nerves in the rat. J Comp Neurol **222,** 473, 1984.
42. Gao, M.Y., Lu, P., Bednark, B., Lynam, D., Conner, J.M., Sakamoto, J., and Tuszynski, M.H. Templated agarose scaffolds for the support of motor axon regeneration into sites of complete spinal cord transection. Biomaterials **34,** 1529, 2013.

43. Schmalenberg, K.E., and Uhrich, K.E. Micropatterned polymer substrates control alignment of proliferating Schwann cells to direct neuronal regeneration. Biomaterials **26,** 1423, 2005.
44. Wen, X., and Tresco, P.A. Effect of filament diameter and extracellular matrix molecule precoating on neurite outgrowth and Schwann cell behavior on multifilament entubulation bridging device in vitro. J Biomed Mater Res A **76,** 626, 2006.
45. Karafyllidis, I.G., and Lagoudas, D.C. Microtubules as mechanical force sensors. Biosystems **88,** 137, 2007.
46. Ellisman, M.H. Beyond neurofilaments and microtubules. Neurosci Res Program Bull **19,** 43, 1981.
47. Hursh, J.B. Conduction velocity and diameter of nerve fibers. Am J Physiol **127,** 131, 2013.
48. Ouyang, H., Nauman, E., and Shi, R.Y. Contribution of cytoskeletal elements to the axonal mechanical properties. J Biol Eng **7,** 21, 2013.
49. Mitchison, T., and Kirschner, M. Cytoskeletal dynamics and nerve growth. Neuron **1,** 761, 1988.
50. Peter, S.J., and Mofrad, M.R.K. Computational modeling of axonal microtubule bundles under tension. Biophys J **102,** 749, 2012.
51. Kidd, G.J., Ohno, N., and Trapp, B.D. Biology of Schwann cells. Handb Clin Neurol **115,** 55, 2013.
52. Beighley, R., Spedden, E., Sekeroglu, K., Atherton, T., Demirel, M.C., and Staii, C. Neuronal alignment on asymmetric textured surfaces. Appl Phys Lett **101,** 143701, 2012.
53. Dowell-Mesfin, N.M., Abdul-Karim, M.A., Turner, A.M., Schanz, S., Craighead, H.G., Roysam, B., Turner, J.N., and Shain, W. Topographically modified surfaces affect orientation and growth of hippocampal neurons. J Neural Eng **1,** 78, 2004.
54. Park, J., Koito, H., Li, J.R., and Han, A. Microfluidic compartmentalized co-culture platform for CNS axon myelination research. Biomed Microdevices **11,** 1145, 2009.
55. Solanki, A., Chueng, S.T.D., Yin, P.T., Kappera, R., Chhowalla, M., and Lee, K.B. Axonal alignment and enhanced neuronal differentiation of neural stem cells on graphene-nanoparticle hybrid structures. Adv Mater **25,** 5477, 2013.
56. Paivalainen, S., Nissinen, M., Honkanen, H., Lahti, O., Kangas, S.M., Peltonen, J., Peltonen, S., and Heape, A.M. Myelination in mouse dorsal root ganglion/Schwann cell cocultures. Mol Cell Neurosci **37,** 568, 2008.
57. Lee, S., Leach, M.K., Redmond, S.A., Chong, S.Y.C., Mellon, S.H., Tuck, S.J., Feng, Z.Q., Corey, J.M., and Chan, J.R. A culture system to study oligodendrocyte myelination processes using engineered nanofibers Nat Methods **9,** 917, 2012.

Address correspondence to:
Christina Chan, PhD
Department of Chemical Engineering
and Materials Science
Michigan State University
East Lansing, MI 48824

E-mail: krischan@egr.msu.edu

Received: July 13, 2015
Accepted: November 5, 2015
Online Publication Date: January 7, 2016